

3-D Frequency Selective Rasorber: Concept, Analysis, and Design

Zhongxiang Shen, *Senior Member, IEEE*, Jiang Wang, and Bo Li

Abstract—This paper introduces the concept, theory, and design of 3-D frequency selective rasorbers (FSRs), which have a transmission window transparent to the incident electromagnetic wave with two absorption bands located at both sides of the window. The proposed rasorber consists of a 2-D periodic array of parallel waveguides. The transmission characteristics with high selectivity are produced by lossless resonators implemented using a parallel waveguide with a metallic post in the center. On the other hand, the absorption bands are obtained by lossy resonators constructed by loading of lumped resistors at the entry port of short-circuited waveguides. Physical mechanism of the proposed FSRs is explained with the aid of an equivalent circuit model, and relevant design equations are formulated. Two prototypes of the designed FSRs are fabricated and measured as a proof of concept. The experimental results show that a bandwidth of 50% for the insertion loss less than 3 dB and two absorption bands with a high absorptance of around 90% can be achieved. Moreover, the simulated results also show that the proposed structure exhibits stable performance against the variation of the incident angle of an incoming plane wave.

Index Terms—Absorber, equivalent circuit model, frequency selective rasorber (FSR), frequency selective surface (FSS).

I. INTRODUCTION

FREQUENCY selective surfaces (FSSs) are spatial filters for electromagnetic (EM) waves, which have found numerous applications due to their attractive frequency filtering characteristics [1]–[3]. These spatial filters can be designed to exhibit bandpass or bandstop response, while the bandpass surfaces are more widely used. Usually, bandpass FSSs strongly reject the incident wave outside the passband resulting in a large radar cross section (RCS), while they allow the wave to pass through without much loss in the passband. In order to maintain the transmission transparency in the passband and reduce the RCS of an FSS-coated object outside the passband, a new class of structures, termed as frequency selective rasorbers (FSRs), was recently reported [4].

Manuscript received January 31, 2016; revised July 5, 2016 and August 26, 2016; accepted August 26, 2016. Date of publication September 16, 2016; date of current version October 4, 2016. An earlier version of this paper was presented at the 2015 Asia-Pacific Microwave Conference, Nanjing, China, Dec. 6–9, 2015.

Z. Shen is with the School of Electrical and Electronic Engineering, Nanyang Technological University, Singapore 639798 (e-mail: ezxshen@ntu.edu.sg).

J. Wang is with the School of Electronic and Optical Engineering, Nanjing University of Science and Technology, Nanjing 210094, China (e-mail: wangjiang923@126.com).

B. Li is with the School of Electronic Science and Engineering, Nanjing University of Posts and Telecommunications, Nanjing 210003, China (e-mail: elibo@njupt.edu.cn).

Color versions of one or more of the figures in this paper are available online at <http://ieeexplore.ieee.org>.

Digital Object Identifier 10.1109/TMTT.2016.2604385

Such FSRs should have a transmission window of low insertion loss to allow the incident waves in the passband to pass through the structure, while they absorb the incident waves at frequencies outside the passband leading to a small RCS. Therefore, an FSR can be seen as a combination of FSS and absorber [5]–[7]. Owing to its unique characteristics, an FSR is very useful in applications that require a transparent frequency window and low RCS outside the transmission window, which is particularly suitable for antenna radomes with low RCS. It may also be useful in systems where mutual interference must be reduced among different subsystems.

In the past, an FSR was realized by cascading a lossy array of Jaumann or circuit analog absorber [8] and a lossless FSS [9], where the transmission characteristic was provided by the conventional FSSs, while the absorption is achieved by the lossy array, such as resistive cross dipoles [10], [11], resistive square loops [12], [13], resistive patches [14], resistor-loaded metallic double-square loops [15]–[17], and indium-tin-oxide film [18]. However, these common FSRs suffer from large unit-cell size and unstable filtering responses over a broad frequency range or large range of incident angle. Moreover, most of the existing FSRs feature lower selectivity for the transmission window together with a low absorption in the rejection band. It is noted that most FSRs exhibit one absorption band only above the transmission window because it is difficult for 2-D FSSs to construct multimode resonators resulting in multiple absorption bands at both sides of the transmission window.

Recently, a class of 3-D FSSs consisting of a 2-D periodic array of multimode resonators was proposed [19]–[22]. Although the implementation of these 3-D FSSs is more complicated compared with traditional 2-D FSS, they can readily achieve high selectivity and angular stable performance. In addition, the unit-cell size and thickness of 3-D FSSs can be designed much smaller than the operating wavelength. An initial FSR based on 3-D FSS was reported in [23]. Unfortunately, the proposed FSR only has an absorption band above the passband, and there is no absorption at frequencies below the passband. On the other hand, the proposed structure in [23] suffers from a relatively large transmission loss in the passband.

This paper presents a new concept of 3-D FSR based on a 2-D periodic array of multimode cavities [22], [24]. An equivalent circuit model is proposed to understand the operating principle, and the corresponding theoretical formulation is provided to reveal the design of the proposed 3-D FSR. After that, two FSRs, one single-polarized and the

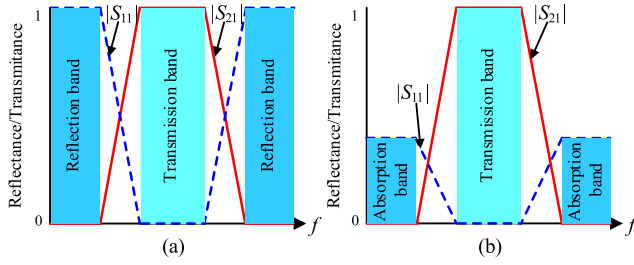


Fig. 1. Reflection and transmission characteristics of an ideal bandpass. (a) FSS. (b) FSR.

other dual-polarized, are designed to verify the design concept. The experimental results demonstrate that both FSRs exhibit a high selectivity with two absorption bands located at both sides of the transmission window. Furthermore, the simulation results verify that the proposed 3-D FSRs exhibit stable filtering and absorption performance for the incident angle up to 40° .

II. CONCEPT

Fig. 1(a) shows the filtering response of a typical bandpass FSS. It exhibits strong reflection at the frequencies out of the passband, which may unavoidably lead to a large RCS when the FSS is coated on an object. In order to reduce the RCS of an FSS-coated target outside the passband, the incident EM waves in the rejection band must be absorbed while maintaining a passband with minimum insertion loss. This is the basic concept of FSR [4], [24]. Fig. 1(b) shows the reflection and transmission characteristics of a typical rasorber. It is seen that a transmission window or passband with minimum insertion loss is produced in the middle, while there are two absorption bands located at both sides of the transmission window. It is clear that both reflection and transmission coefficients are small outside the passband due to the absorption introduced.

Fig. 2 shows a conceptual design of a 3-D FSR consisting of a 2-D periodic array of multimode cavities. Based on the key concept 3-D FSS, the multimode cavity in a unit cell is usually a guided-wave structure [25], such as a shielded microstrip line [19], or any other suitable geometry [26]. Multiple propagation modes in a unit cell are excited by the incident EM wave, and multimode resonators are then constructed in a single cell. By controlling the number of resonators and their couplings with the incident plane wave in free space, a desired frequency response can be obtained [19]. In order to realize an FSR, a lossless resonator must be constructed to transmit the EM wave through the guided-wave structure with open circuit at both ends of the resonator. On the other hand, lossy resonators are constructed to absorb the incident plane wave by loading lumped resistors into the resonators whose resonant frequencies are located outside the passband. Employing this concept, it is then possible to obtain dual absorption bands at both sides of a passband using three resonators: a lossless resonator resonating at the center frequency f_C and two lossy resonators resonating at lower and higher frequencies f_L and f_U , respectively. Here, f_C , f_L , and f_U denote the center frequencies in the passband as well

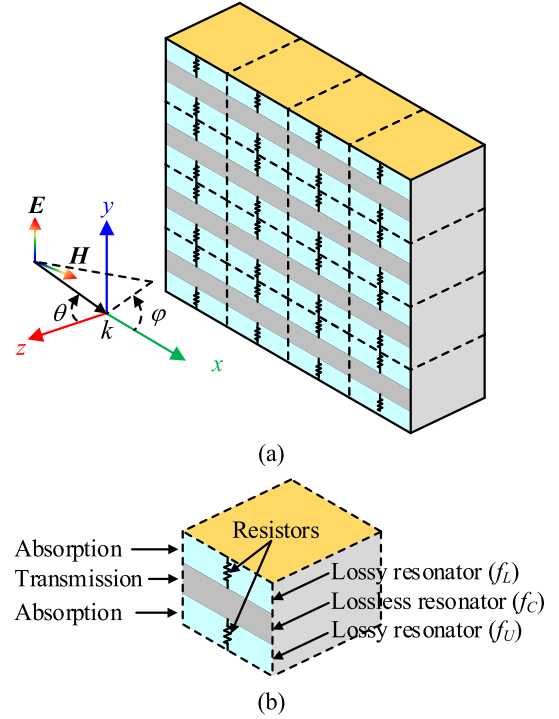


Fig. 2. Illustration of a 3-D FSR consisting of a 2-D periodic array of multimode cavities.

as the lower and upper absorption bands, respectively. At f_C , the reflection coefficient should be zero and its corresponding transmission coefficient should be equal to one, whereas at the frequencies of f_L and f_U , both reflection and transmission coefficients are ideally equal to zero.

Since the lossy resonator operating at the lower frequency will unavoidably produce harmonics at higher frequencies, we are able to use these harmonics to realize the upper band absorption. In other words, the lossy resonator operating at higher frequencies (f_U) may not be necessary in a simplified design. Based on this consideration, we can use two resonators to realize a rasorber: one lossless for the transmission window and the other lossy resonator to obtain dual-band absorption at both sides of the passband. Such a simplified design will be analyzed in the next section, and its design guidelines will also be formulated.

III. ANALYSIS AND DESIGN

Fig. 3(a) shows a unit cell of the proposed 3-D FSR consisting of two parallel-plate waveguide sections and its corresponding equivalent circuit model. The unit cell contains only one lossless resonator and another lossy resonator, which provide the transmission and absorption bands, respectively. It should be pointed out that the polarization direction of the incoming plane wave is vertical for this design, while a dual-polarized design will be discussed in Section V. The equivalent circuit model of the structure can be divided into two subnetworks, representing the absorption and propagation paths, respectively. In the absorption path, the lossy resonator is equivalent to a short-circuited transmission line section (Z_a , θ_a) with a lumped resistor connected at the input port, as shown in Fig. 3(b). However, the lossless resonator can be

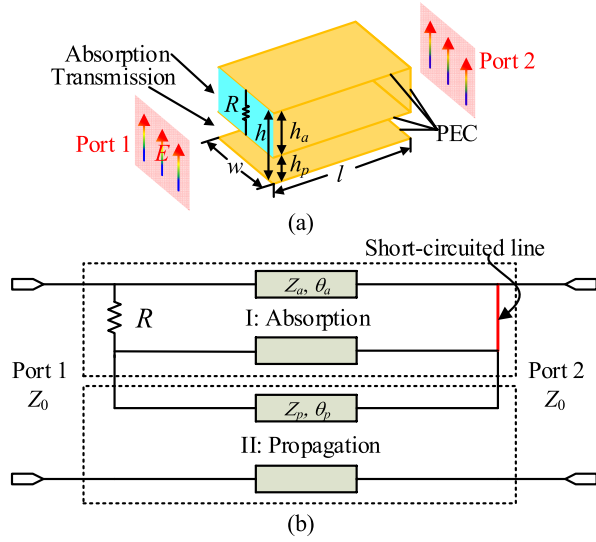


Fig. 3. Unit cell of the proposed 3-D FSR and its corresponding equivalent circuit model.

represented as a transmission-line section (Z_p, θ_p) with open circuit at both terminals.

According to the above equivalent circuit model, the impedance parameters of these two subnetworks can be expressed, respectively, as

$$Z_I = \begin{pmatrix} jRZ_a \tan \theta_a / (R + jZ_a \tan \theta_a) & 0 \\ 0 & 0 \end{pmatrix} \quad (1)$$

$$Z_{II} = \begin{pmatrix} -jZ_p / \tan \theta_p & -jZ_p / \sin \theta_p \\ -jZ_p / \sin \theta_p & -jZ_p / \tan \theta_p \end{pmatrix}. \quad (2)$$

The characteristic impedances ($Z_a = \eta_0 h_a / w$ and $Z_p = \eta_0 h_p / w$, where $\eta_0 = 377\Omega$ is the wave impedance in free space) and electrical lengths ($\theta_a = \theta_p = 2\pi l / \lambda$, where λ is the free-space wavelength) of the absorption and propagation paths can be obtained from the physical dimensions. By connecting these two subnetworks in series, the impedance parameters of the entire equivalent circuit model can be written as follows:

$$Z = Z_I + Z_{II}. \quad (3)$$

After the impedance matrix of the equivalent circuit model shown in Fig. 3 is obtained, closed-form expressions for all the four scattering parameters of the structure can be analytically derived [27]

$$S_{11} = \frac{(Z_{11} - Z_0)(Z_{22} + Z_0) - Z_{12}Z_{21}}{\Delta Z} \quad (4)$$

$$S_{12} = \frac{2Z_{12}Z_0}{\Delta Z} \quad (5)$$

$$S_{21} = \frac{2Z_{21}Z_0}{\Delta Z} \quad (6)$$

$$S_{22} = \frac{(Z_{11} + Z_0)(Z_{22} - Z_0) - Z_{12}Z_{21}}{\Delta Z} \quad (7)$$

where $\Delta Z = (Z_{11} + Z_0)(Z_{22} + Z_0) - Z_{12}Z_{21}$, and $Z_0 = \eta_0 h / w$ is the characteristic impedance of the parallel-plate waveguide.

In order to illustrate the operating principle of the proposed structure and gain insight into the transmission and absorption mechanisms, three special cases are discussed as follows.

- 1) At f_L , $l = \lambda_L / 4$ and $\theta_a = \theta_p = \pi / 2$. Both transmission line sections are of a quarter wavelength, and they can transform open circuit to short circuit, and vice versa. Therefore, the quarter-wavelength transmission line terminated with short circuit is equivalent to an open circuit. On the other hand, the quarter-wavelength transmission line terminated with an open circuit or large load impedance for the free space has an input impedance equal to Z_p^2 / Z_0 , where Z_0 is the wave impedance for free space. Therefore, the whole input impedance Z_{in} at Port 1 is equal to $R + Z_p^2 / Z_0$. The impedance matching ($Z_{in} = Z_0$) can be easily obtained by properly choosing the values of the loaded resistor. In this case, the reflection coefficient $|S_{11}|$ is ideally equal to zero and the transmittance $|S_{21}|$ is approximately equal to zero, which means that the incident wave will be substantially absorbed.
- 2) At the frequency of $f_C = 2f_L$, $l = \lambda_C / 2$ and $\theta_a = \theta_p = \pi$. Under this situation, both transmission line sections are of half a wavelength. It is known that the input impedance of a terminated half-wavelength transmission line is exactly equal to the load impedance, regardless of its characteristic impedance. Since the absorption path is a short-circuited transmission line, the loaded resistor will be bypassed as it is in shunt connection with a short circuit. The input impedance of the transmission path is Z_0 since its length is also half a wavelength. Therefore, the overall input impedance Z_{in} at Port 1 of the equivalent model is equal to Z_0 , which produces a perfect transmission. $S_{11} = 0$, and $S_{21} = 1$. This is the required transmission window ideally with zero insertion loss.
- 3) At $f_U = 3f_L$, $l = 3\lambda_U / 4$ and $\theta_a = \theta_p = 3\pi / 2$. Both transmission sections are of three quarters of a wavelength at this frequency. This situation is basically the same as 1), which gives the overall input impedance $Z_{in} = R + Z_p^2 / Z_0$. Resultantly, the same absorbing properties should be achieved at this upper frequency. In addition, the lossy resonator operating at the lower frequency will produce harmonics at higher frequencies, which means that a high-frequency absorption is inevitable.

Fig. 4 shows the simulated scattering parameters of the structure obtained using HFSS full-wave simulations and theoretical analysis based on the equivalent circuit model. It is seen that there exists a significant difference between them for the reflection coefficient ($|S_{11}|$) from 2.5 to 3.7 GHz. The reflection level of the simulated results by HFSS is much higher and reaches to -5 dB. The main reason behind the difference is because the equivalent circuit model ignores step capacitors existing at the discontinuity interfaces between free space and parallel-plate waveguide, which causes a difference in the electric lengths of absorption and transmission patch. In order to compensate for the effect of the step

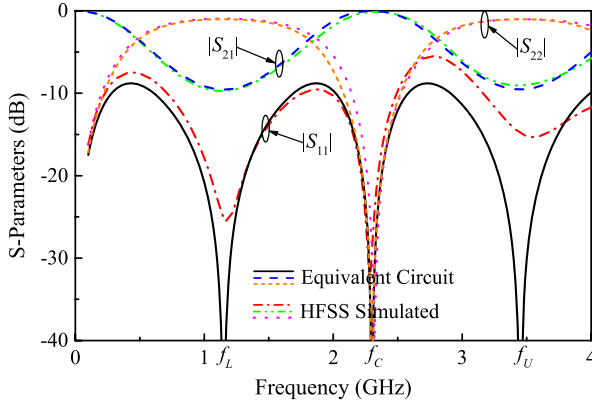


Fig. 4. Comparison of scattering parameters of the designed FSR obtained by HFSS full-wave simulation and from the equivalent circuit model (physical dimensions: $w = h = 21$ mm, $h_a = 14$ mm, $h_p = 7$ mm, $l = 60$ mm, and $R = 335 \Omega$; equivalent circuit parameters: $Z_0 = 377 \Omega$, $Z_a = 251.33 \Omega$, $Z_p = 125.67 \Omega$, $\theta_a = 90^\circ$ at 1.15 GHz, and $\theta_p = 90^\circ$ at 1.15 GHz).

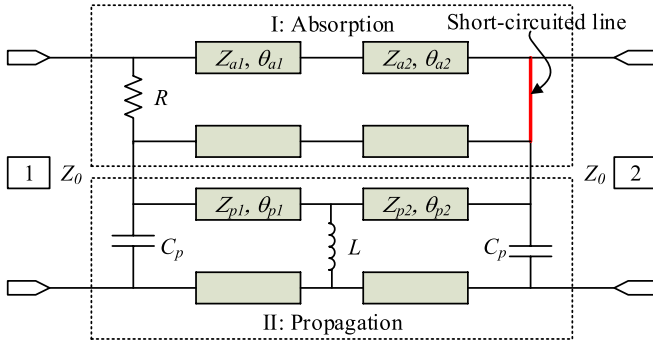


Fig. 5. Equivalent circuit model of the improved FSR.

capacitances, one effective way is to increase the electrical length of the absorption path by inserting a small section of Teflon with a dielectric constant of ϵ_r in the short-circuited parallel-plate waveguide without changing any other parameters.

Moreover, it is seen that the reflection coefficient at Port 2 ($|S_{22}|$) is equal to $|S_{11}|$ in the passband, while it is around 0 dB at frequencies out of the passband. Furthermore, the transmission coefficient ($|S_{21}|$) shown in Fig. 4 exhibits an oscillating variation, which means that the selectivity of this structure is not very good. In order to improve the filtering characteristics of the structure, a metallic post can be introduced at the center of the propagation path to link the middle and bottom layers [21]. This post can be represented by an inductor in the equivalent circuit model. Based on the above considerations, the improved equivalent circuit model is given in Fig. 5. The upper layer waveguide structure, partially filling with Teflon, can be regarded as two cascaded transmission-line sections: (Z_{a1}, θ_{a1}) and (Z_{a2}, θ_{a2}) . For the bottom layer structure, two discontinuity capacitors are added at both sides, and the original transmission line (Z_p, θ_p) is separated into two sections: (Z_{p1}, θ_{p1}) and (Z_{p2}, θ_{p2}) , by inserting an inductor at the middle. C_p and L denote the step capacitance and via inductance, respectively.

The transfer matrices of these two subnetworks can be calculated, respectively, as

$$\begin{pmatrix} A_I & B_I \\ C_I & D_I \end{pmatrix} = \begin{pmatrix} 1 & 0 \\ 1/R & 1 \end{pmatrix} \begin{pmatrix} \cos \theta_{a1} & jZ_{a1} \sin \theta_{a1} \\ j \sin \theta_{a1}/Z_{a1} & \cos \theta_{a1} \end{pmatrix} \times \begin{pmatrix} \cos \theta_{a2} & jZ_{a2} \sin \theta_{a2} \\ j \sin \theta_{a2}/Z_{a2} & \cos \theta_{a2} \end{pmatrix} \begin{pmatrix} 1 & 0 \\ \infty & 1 \end{pmatrix} \quad (8)$$

$$\begin{pmatrix} A_{II} & B_{II} \\ C_{II} & D_{II} \end{pmatrix} = \begin{pmatrix} 1 & 0 \\ jwC_p & 1 \end{pmatrix} \begin{pmatrix} \cos \theta_{p1} & jZ_{p1} \sin \theta_{p1} \\ j \sin \theta_{p1}/Z_{p1} & \cos \theta_{p1} \end{pmatrix} \times \begin{pmatrix} 1 & 0 \\ 1/jwL & 1 \end{pmatrix} \times \begin{pmatrix} \cos \theta_{p2} & jZ_{p2} \sin \theta_{p2} \\ j \sin \theta_{p2}/Z_{p2} & \cos \theta_{p2} \end{pmatrix} \begin{pmatrix} 1 & 0 \\ jwC_p & 1 \end{pmatrix} \quad (9)$$

where $w = 2\pi f$ and f is the operating frequency. The characteristic impedances (Z_{a1} , Z_{a2} , Z_{p1} , and Z_{p2}) and electrical lengths (θ_{a1} , θ_{a2} , θ_{p1} , and θ_{p2}) of the absorption and propagation paths can be obtained from their physical dimensions. Moreover, the capacitance C_p can be estimated as [28]

$$C_p \approx \frac{1}{\omega X_p} = \frac{h}{\omega h_p Z_0} \tan \varphi \quad (10)$$

where

$$\varphi = \frac{2h}{\lambda} \left(\frac{h_a}{h} \ln \frac{h}{h_a} + \frac{h_p}{h} \ln \frac{h}{h_p} \right) + S \left(\frac{2h}{\lambda} \right) - S \left(\frac{2h_a}{\lambda} \right) - S \left(\frac{2h_p}{\lambda} \right) \quad (11)$$

and $S(x) = \sum_{n=1}^{\infty} (\arcsin(x/n) - x/n)$. Furthermore, the inductance L is expressed as [29]

$$L = \frac{\mu_0 h_p}{2\pi} [\ln(4h_p/d) + d/(2h_p) - 1]. \quad (12)$$

We can then obtain the impedance matrices Z_I and Z_{II} of the absorption and propagation paths through the simple conversion between $ABCD$ matrices and Z matrices [27]. Finally, the corresponding scattering parameters can be obtained through (3)–(7). Based on the above considerations and theoretical analysis, two FSRs are presented in the next two sections: one is single polarized and the other is dual polarized.

IV. SINGLE-POLARIZED FSR

Fig. 6 shows the geometrical details of our proposed single-polarized FSR. Each unit cell of the FSR consists of three copper sheets (their thickness t_m is assumed to be negligible compared with the operating wavelength); they form two parallel-plate waveguides: one short circuited and the other open circuited. Due to the existence of two parallel-plate waveguide sections, two distinct channels are naturally formed: the open-circuited one is for the passband and the other short-circuited one loaded with a shunt resistor at its input port is for the absorption band. It is seen that a metallic post is soldered at the center of the open path, which helps to produce a sharp rolloff performance of the transmission window.

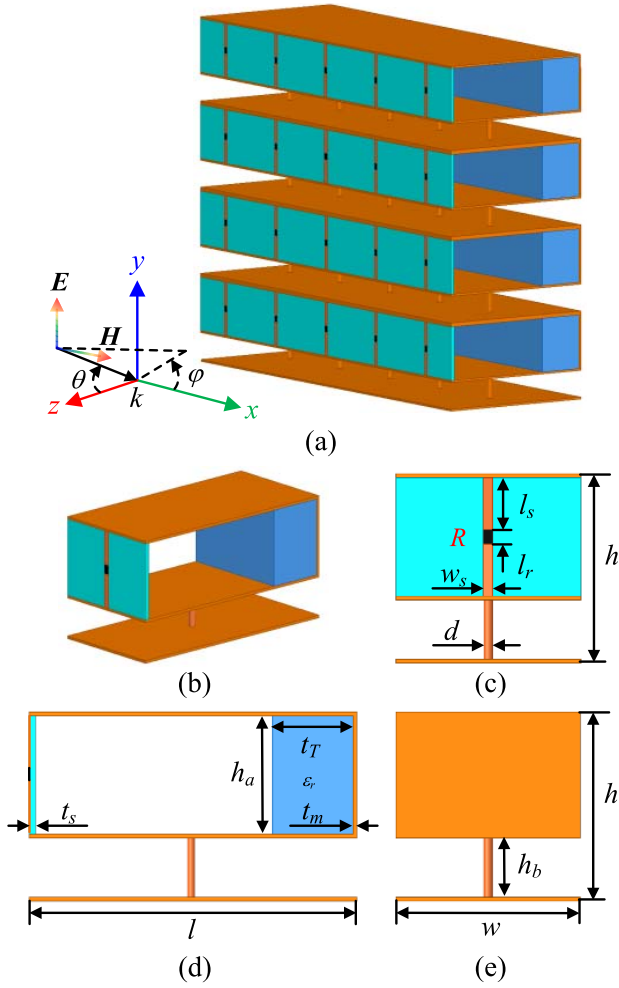


Fig. 6. Geometry of the proposed single-polarized FSR. (a) 3-D view of the FSR. (b) Perspective, (c) front, (d) side, and (e) backside view of a unit cell of the FSR. (Physical dimensions: $w = 22.5$ mm, $w_s = 0.5$ mm, $t_s = 0.508$ mm, $t_m = 0.5$ mm, $t_T = 22$ mm, $d = 0.5$ mm, $h = 22.5$ mm, $h_a = 14$ mm, $h_p = 7$ mm, $l = 60$ mm, $l_s = 6.5$ mm, $l_r = 1$ mm, $R = 330 \Omega$, and $\epsilon_r = 2.1$; corresponding equivalent circuit parameters: $Z_0 = 377 \Omega$, $Z_{a1} = 247 \Omega$, $Z_{a2} = 170 \Omega$, $Z_{p1} = Z_{p2} = 130 \Omega$, $C_p = 0.02$ pF, $L = 4.2$ nH, $\theta_{a1} = 90^\circ$ at 1.82 GHz, $\theta_{a2} = 90^\circ$ at 2.16 GHz, $\theta_{p1} = 90^\circ$ at 2.3 GHz, and $\theta_{p2} = 90^\circ$ at 2.3 GHz.)

It is also seen that the vertical single-layer strip line is introduced to connect the lumped resistor to construct the lossy resonators, which can absorb the incident plane waves at the frequencies below and above the passband. Furthermore, a short section of rectangular Teflon is inserted into the short-circuited parallel-plate waveguide to slightly extend its electrical length. Fig. 6(a) also indicates that the proposed FSR functions well only for y -polarized incident wave, where k and (ϕ, θ) denote the propagation direction and incidence azimuth angle of the incident wave, respectively.

Fig. 6(b)–(e) illustrates the structural details of a unit cell. It is seen that a single-layer circuit board, containing two strip lines linked by a lumped resistor, is vertically placed at the left side of the horizontal copper sheets. At the right side, a short metallic surface connects the upper and middle copper sheets, which form a short circuit. In addition, a post of diameter d is in contact with the middle and bottom copper sheets, which is utilized to split the resonant frequency so as to obtain a

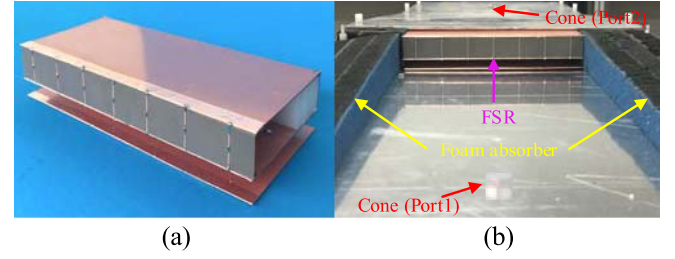


Fig. 7. (a) Photograph of the fabricated single-polarized FSR. (b) Measurement setup.

higher selectivity for the filtering response. The thickness of the proposed FSR is denoted by l . The unit cell of the FSR is simulated by the full-wave EM simulation software *ANSYS HFSS*. The periodic boundary conditions *Master* and *Slave* are adopted along the x and y directions to simulate the infinitely large periodic structure. The unit cell periods along the x and y directions are denoted by w and h , respectively.

Based on the understanding gained in the previous sections, it is concluded that a passband with two transmission poles is produced by two lossless resonators R_1 and R_2 in the propagation path. The transmission zeros below and above the passband are produced by the lossy resonator R_L and its first harmonic formed by the single-layer air-filled parallel-plate waveguide section loaded with a resistor at its input and a short-circuited Teflon-filled waveguide section at its output. Therefore, a transmission window with high selectivity is obtained, while the lower and upper absorption bands are achieved in the meanwhile.

A prototype of the designed single-polarized FSR is fabricated and measured. Fig. 7(a) shows the photograph of our fabricated sample, which contains seven unit cells along the horizontal direction. The single-layer strip lines are printed on a substrate of Rogers 5880 with a dielectric constant of 2.2 and a thickness of 0.508 mm, where lumped resistors are soldered in between and are in good contact with the copper sheets. It is also noted that Vishay 71-FC0402E3300DTWS resistors are used in the fabricated sample, which are very close to the theoretical resistance value of 335Ω . The geometrical parameters of the FSR are listed in the caption of Fig. 6. The fabricated sample is measured in a parallel-plate waveguide, as shown in Fig. 7(b), which is similar to the measurement setup described in [15].

Fig. 8(a) shows the comparison of measured, simulated, and equivalent circuit model calculated transmission and reflection coefficients of the proposed single-polarized FSR under the normal incidence. It should be pointed out that the lowest operating frequency of the waveguide test system is 1 GHz, which limits our lowest measured frequency at 1 GHz. It is clear that a good agreement between measured, simulated, and calculated results is obtained and the small difference between them is attributed to the fabrication and measurement errors. In addition, Fig. 8(a) exhibits that a transmission window with insertion loss less than 3 dB is obtained for the frequency range from 1.5 to 2.5 GHz, representing a fractional bandwidth of 50% at the center frequency of 2 GHz. The sharp rolloff edges at both sides are attributed to the introduced posts. Furthermore, Fig. 8(a) shows that the reflection coefficient

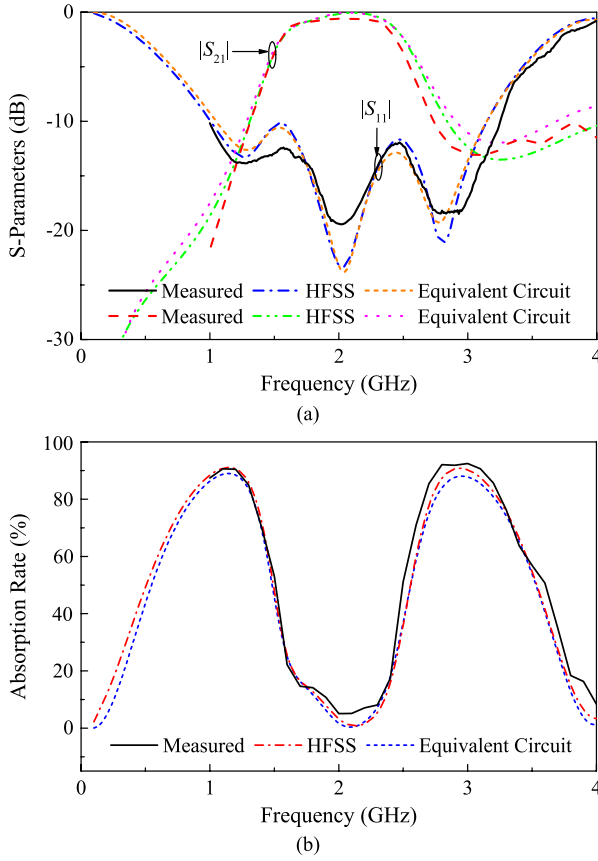


Fig. 8. Measured, simulated, and calculated performance of the single-polarized FSR under the normal incidence. (a) Scattering parameters. (b) Absorption spectrum.

is below -10 dB from 0.95 to 3.3 GHz, which is much wider than the bandwidth of the passband. It is expected that the incident wave is mostly absorbed by the structure at the frequency from 0.95 to 1.5 and 2.5 to 3.3 GHz.

Correspondingly, the absorption spectrum of the proposed single-polarized FSR is plotted in Fig. 8(b). It can be seen that two absorption bands with a high absorptivity of around 90% can be obtained. The frequency for the absorption rate larger than 80% is from 0.84 to 1.35 and 2.73 to 3.29 GHz, representing a fractional bandwidth of 46.6% and 18.6% with respect to the center frequencies of 1.1 and 3.01 GHz, respectively. It is worth pointing out that the high selectivity of absorption corresponds to the good filtering response, and the absorption bands are separately located at both sides of the transmission window.

The frequency responses of the singly polarized FSR under oblique incidence are investigated. Figs. 9 and 10 show the simulated performance when the incident angle θ scans in the xz and yz planes, respectively. It is observed that the bandpass filtering characteristic of our FSR is stable under different incident angles. It is also seen in Fig. 9(a) that the transmission windows slightly shift to a higher frequency with the increasing incident angle. This variation with respect to the incident angle is attributed to the change of the electrical lengths of the waveguide sections viewed from the oblique incident angle. Therefore, when enlarging the incident angle, a smaller effective electrical length is obtained, and

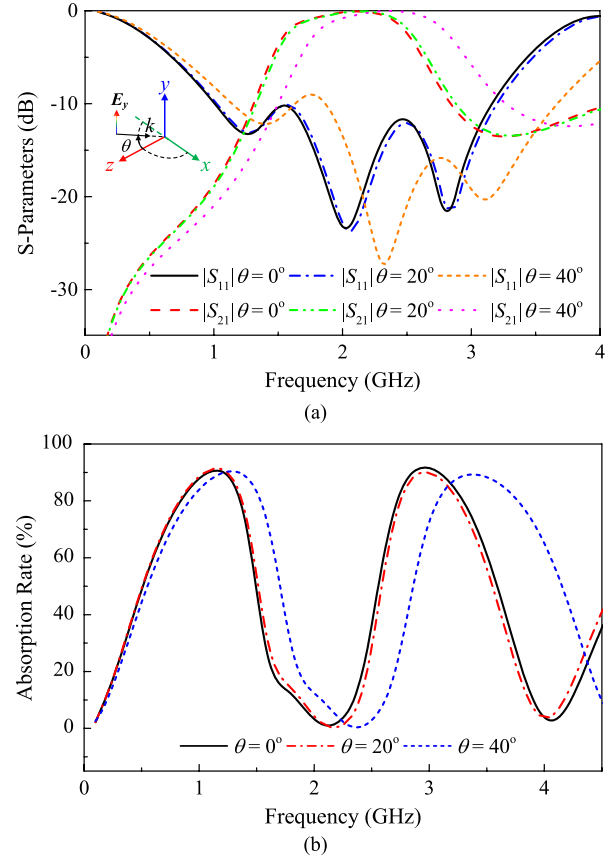


Fig. 9. Simulated performance of the single-polarized FSR under oblique incidence in the xz plane ($0^\circ, \theta$). (a) Reflection and transmission coefficients. (b) Absorption spectrum.

the center frequency will unavoidably shift to the higher frequency. Correspondingly, when the incident angle increases from 0° to 40° , the simulated bandwidth for absorption rate larger than 80% varies from 46.6% to 49.8% and from 18.6% to 20%, respectively, as seen in Fig. 9(b). In addition, Fig. 10 exhibits that the performance under oblique incidence in the yz plane ($90^\circ, \theta$) is more stable compared with the xz plane ($0^\circ, \theta$). Moreover, the reflection coefficient slightly increases while the transmission coefficient decreases, which is due to the impedance mismatching under oblique incidence. Furthermore, the absorption rate shown in Fig. 10(b) does not change much for different incident angles ($90^\circ, \theta$) although some degradations occur at the upper absorption band.

V. DUAL-POLARIZED FSR

Fig. 11 provides the geometrical details of the proposed dual-polarized FSR, which is modified from the single-polarized FSR described in the previous section. It is noted that this structure can function well for both x - and y -polarized incident plane waves. In this design, the lossy resonators are constructed using an array of individual quadripole folded copper sheets and a small Teflon square cylinder is inserted in the center near the end. A double-layer circuit board loaded with two lumped resistors on both sides is vertically placed on the left side of the structure. The propagation paths are distributed around the absorption paths, which are formed by the parallel-plate waveguides inserted with metallic posts.

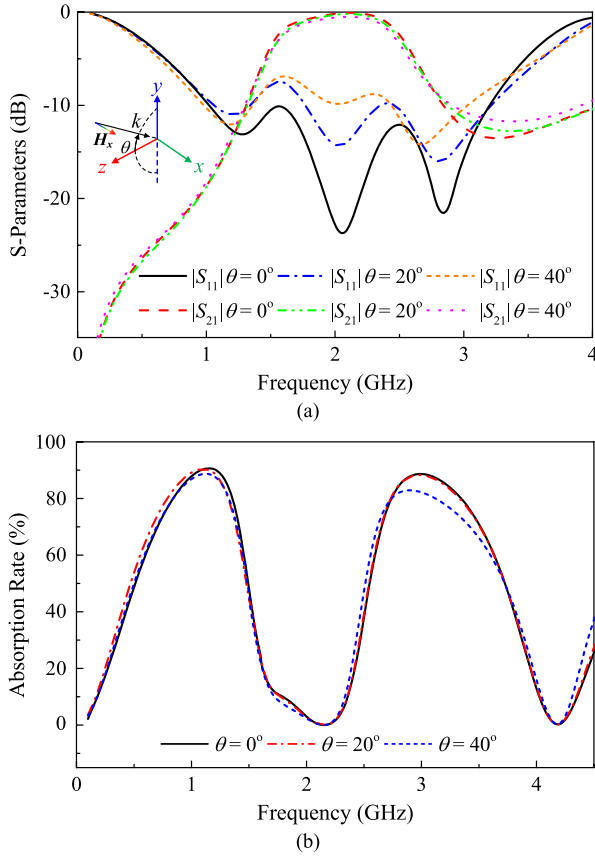


Fig. 10. Simulated performance of the single-polarized FSR under oblique incidence in the yz plane ($90^\circ, \theta$). (a) Reflection and transmission coefficients. (b) Absorption spectrum.

The structural details of a unit cell of the dual-polarized FSR are shown in Fig. 11(b)–(e). It can be seen that the structure is symmetrical, which ensures that the dual-polarized FSR has the same performance under both parallel and perpendicular polarizations. It is noted that the double-layer circuit board, containing two perpendicular strip lines linked by lumped resistors for each layer, is soldered to the left side of the folded copper sheets. The wave reflected by the short-circuited transmission line section on the other side will be absorbed by the resistors at the input side. The bandpass filtering response is obtained from the air gap between the quadripole folded copper sheets with the height indicated as h_p . The unit cell has the same period w along the x - and y -axis. The simulation of this unit cell is the same as the pervious single-polarized FSR.

Simulated reflection coefficient, transmission coefficient, and absorption rate of the proposed dual-polarized FSR for both x - and y -polarized incident waves under the normal incidence are shown in Fig. 12. It is obvious that all corresponding curves nearly overlap each other, which clearly demonstrates that the structure has identical performance for x - and y -polarization. Hence, the experimental verification is carried out under only one polarization.

In order to verify the proposed design, a sample of the designed dual-polarized FSR is fabricated and measured. Fig. 13 shows the photograph of our fabricated sample, which contains six unit cells along the horizontal axis. The bottom thin foam board is utilized to support the whole structure,

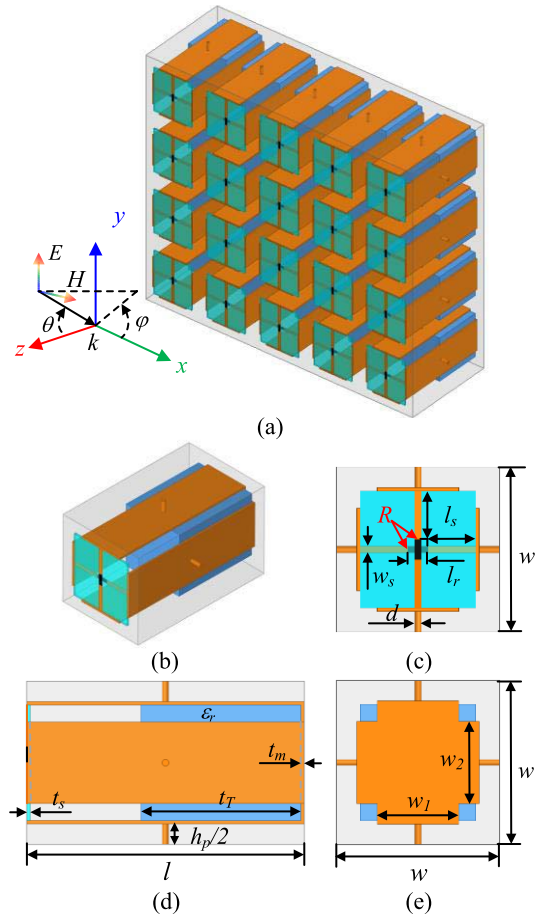


Fig. 11. Schematic of the proposed dual-polarized FSR. (a) 3-D view of the FSR. (b) Perspective, (c) front, (d) side, and (e) backside view of a unit cell of the FSR. (Physical dimensions: $w = 24$ mm, $w_s = 0.5$ mm, $w_1 = w_2 = 10$ mm, $t_s = 0.508$ mm, $t_m = 0.5$ mm, $t_T = 26$ mm, $d = 0.5$ mm, $h_p = 6.4$ mm, $l = 60$ mm, $l_s = 7.8$ mm, $l_r = 1$ mm, $R = 330 \Omega$, and $\epsilon_r = 2.1$.)

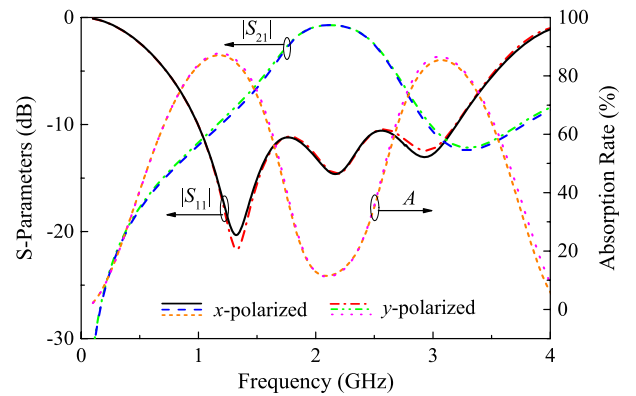


Fig. 12. Simulated performance of the dual-polarized FSR under the normal incidence for both x - and y -polarized incident waves.

while the side foam is used to ensure that an identical spacing between two units is maintained. It should be pointed out that the dielectric constant of the foam is very close to one, and therefore their effects can be ignored. Moreover, the double-layer strip lines linked by a lumped resistor are printed on both sides of the substrate, and they are, respectively,

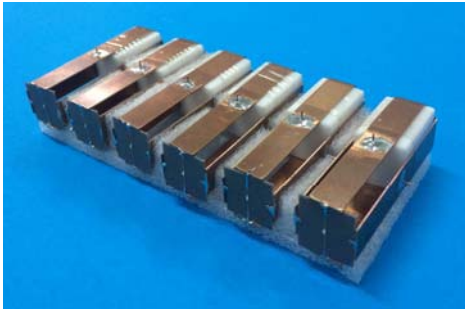


Fig. 13. Photograph of the fabricated dual-polarized FSR.

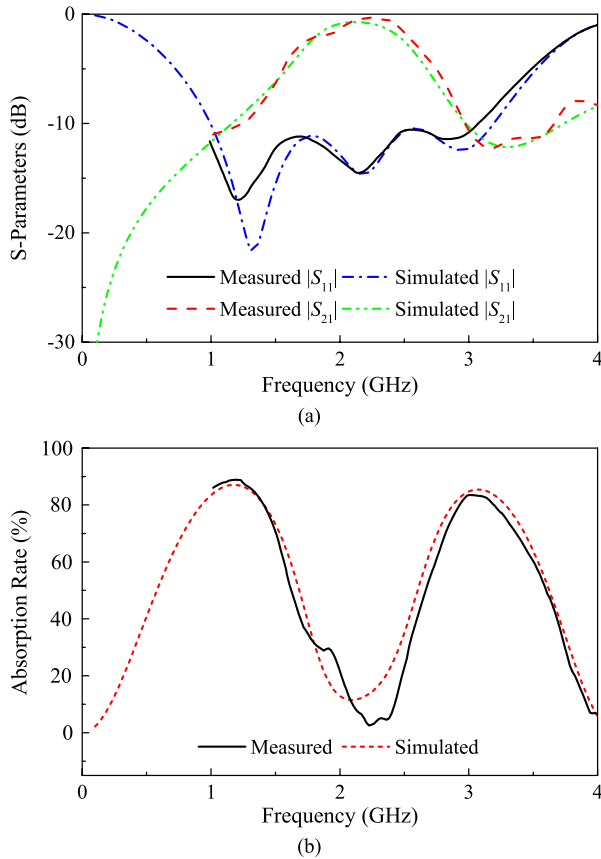


Fig. 14. Measured, simulated, and calculated performance of the dual-polarized FSR under the normal incidence. (a) Scattering parameters. (b) Absorption spectrum.

soldered to the four terminals of the copper sheets, as shown in Fig. 13. The geometrical parameters of the dual-polarized FSR are listed in the caption of Fig. 11. It is worth mentioning that the measurement procedure is the same as the previous single-polarized one.

The comparison of measured and simulated reflection and transmission coefficients of the proposed dual-polarized FSR under the normal incidence is shown in Fig. 14. Good agreement between the measured and simulated results can be observed, while the small difference is attributed to fabrication tolerance. It can be seen in Fig. 14(a) that a passband with insertion loss less than 3 dB is from 1.75 to 2.7 GHz, corresponding to a fractional bandwidth of 43.2% with respect

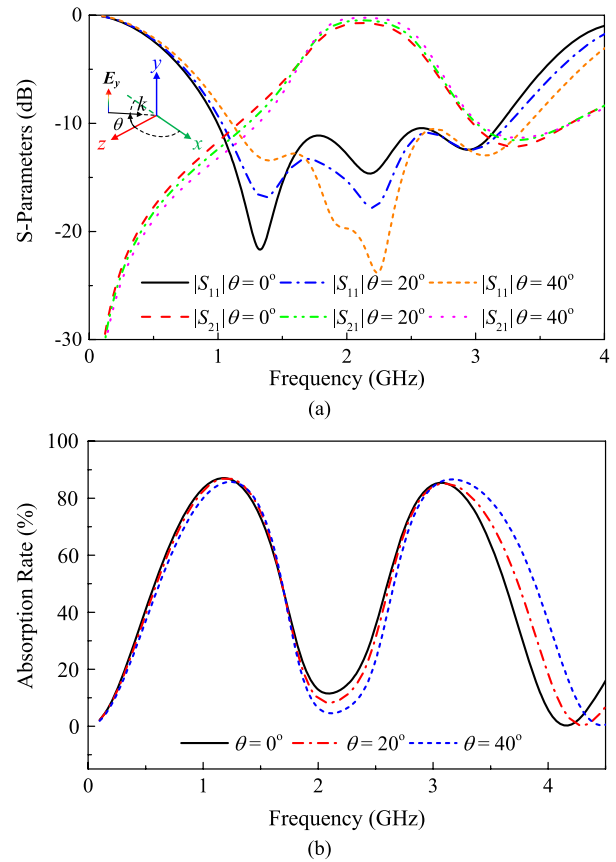


Fig. 15. Simulated performance of the dual-polarized FSR under the oblique incidence in the xz plane ($0^\circ, \theta$). (a) Reflection and transmission coefficients. (b) Absorption spectrum.

to the center frequency of 2.2 GHz. It may be noted that the frequency filtering characteristic is somehow degraded, which is due to the fact that the width of the copper sheets is slightly smaller than the period of the unit cell to avoid the contact between the four terminals. Therefore, the quality factor of the dual-polarized FSR is inevitably reduced compared with the single-polarized FSR and its selectivity performance is accordingly weakened. Moreover, the variation of the reflectivity reveals that a wider reflection bandwidth from 0.95 to 3.2 GHz can be obtained, which indicates that the reflected wave for frequencies from 0.95 to 1.75 and 2.7 to 3.2 GHz will be absorbed by the structure.

The absorption rate of the dual-polarized FSR is shown in Fig. 14(b). Two absorption bands with high absorptivity are observed at both sides of the passband. It is seen that the absorption rate larger than 80% is from 0.92 to 1.43 and 2.84 to 3.31 GHz, representing fractional bandwidths of 43.2% and 15.3% with respect to the center frequencies of 1.18 and 3.08 GHz, respectively.

The performance of our proposed dual-polarized FSR under oblique incidence in the xz and yz planes is also investigated, as shown in Figs. 15 and 16. It is seen that there is little change with an increasing incident angle, and this implies that the proposed dual-polarized FSR exhibits stable performance under the oblique incidence. When the angle of the incident wave varies in the xz plane, it is noted in Fig. 15(a) that the center

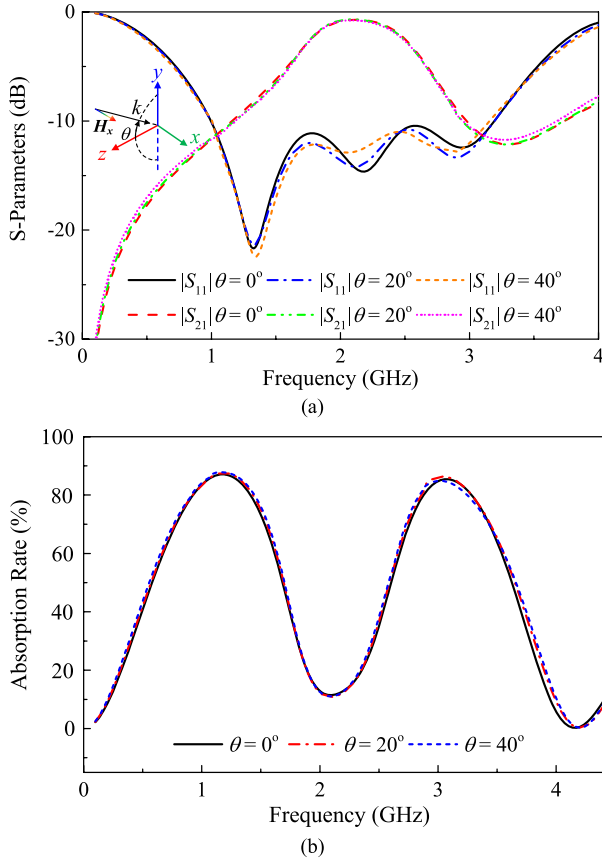


Fig. 16. Simulated performance of the dual-polarized FSR under the oblique incidence in the yz plane ($90^\circ, \theta$). (a) Reflection and transmission coefficients. (b) Absorption spectrum.

TABLE I
PERFORMANCE SUMMARIZATION OF THE PROPOSED FSRs

FSRs	Lower Absorption Band		Transmission Band		Upper Absorption Band	
	Max. Rate	Band-width	Insertion Loss	Band-width	Max. Rate	Band-width
Single-Pol.	93%	46.6%	0.2 dB	50%	90%	18.6%
Dual-Pol.	88%	43.2%	0.5 dB	43.2%	87%	15.3%

frequency slightly shifts toward a higher frequency, similar to the case of the single-polarized FSR. Accordingly, when the incident angle increases from 0° to 40° , the simulated bandwidth of the absorption rate better than 80% varies from 43.2% to 36% and 15.3% to 17.2%, respectively, as seen in Fig. 15(b). In addition, the S -parameters and absorption rate separately shown in Fig. 16(a) and (b) are stable in the yz plane for the incident angle up to 40° .

To clearly demonstrate the performance of our proposed single- and dual-polarized FSRs, a comparison is made in Table I. It is clear that our proposed FSRs have two absorption bands and a transmission band. As shown in Table I, the single-polarized FSR has maximum absorption rates of 93% and 90%, as well as bandwidths (absorption rate better than 80%) of 46.6% and 18.6% for the lower and upper absorption bands, respectively.

Moreover, a bandwidth (transmission coefficient above -3 dB) of 50% and a very low insertion loss of 0.2 dB can be obtained for the single-polarized FSR. Furthermore, the dual-polarized FSR has a similar performance to that of the single-polarized one although all performance indicators are slightly degraded.

VI. CONCLUSION

This paper has introduced the basic design concept of 3-D FSRs that can exhibit a transmission window with very low insertion loss and two absorption bands on both sides of the passband. The rasorber can be implemented using a 2-D periodic array of 3-D unit cells based on two parallel transmission line sections: one section is short circuited at one end and loaded with a lumped resistor at the other end, and the other is a through-line for the transmission window. Analysis formulas and design guidelines have been provided to explain the operating principle of this rasorber. Two design examples for single-polarized and dual-polarized FSRs have been presented, and the measured results are in good agreement with the simulated ones, which validates the proposed design concept. It has been demonstrated that the proposed 3-D FSR features a highly selective filtering response, very low insertion loss in the passband, and two absorption bands located at both sides of the transmission window. It also exhibits stable angular response under the oblique incidence. Further improvements of the proposed FSR include a reduction in its thickness, simplified cell design, and curved FSR.

REFERENCES

- [1] T. K. Wu, *Frequency Selective Surface and Grid Array*. New York, NY, USA: Wiley, 1995.
- [2] B. A. Munk, *Frequency Selective Surfaces: Theory and Design*. New York, NY, USA: Wiley, 2000.
- [3] G. Q. Luo, W. Hong, Q. H. Lai, K. Wu, and L. L. Sun, "Design and experimental verification of compact frequency-selective surface with quasi-elliptic bandpass response," *IEEE Trans. Microw. Theory Techn.*, vol. 55, no. 12, pp. 2481–2487, Dec. 2007.
- [4] B. A. Munk, *Metamaterials: Critique and Alternatives*. Hoboken, NJ, USA: Wiley, 2009.
- [5] A. Motevasselian and B. L. G. Jonsson, "Design of a wideband rasorber with a polarisation sensitive transparent window," *IET Microw. Antenna Propag.*, vol. 6, no. 7, pp. 747–755, May 2102.
- [6] L. Liu, W. Wei, J. Mo, Y. Fu, and N. Yuan, "Analysis of frequency selective surface absorbers via a novel equivalent circuit method," *Chin. Phys. B*, vol. 22, no. 4, pp. 047802-1–047802-5, Apr. 2013.
- [7] R. Panwar, S. Puthucheri, V. Agarwala, and D. Singh, "Fractal frequency-selective surface embedded thin broadband microwave absorber coatings using heterogeneous composites," *IEEE Trans. Microw. Theory Techn.*, vol. 63, no. 8, pp. 2438–2448, Aug. 2015.
- [8] B. A. Munk, P. Munk, and J. Pryor, "On designing Jaumann and circuit analog absorbers (CA absorbers) for oblique angle of incidence," *IEEE Trans. Antennas Propag.*, vol. 55, no. 1, pp. 186–193, Jan. 2007.
- [9] A. Fallahi, A. Yahaghi, H.-R. Benedickter, H. Abiri, M. Shahabadi, and C. Hafner, "Thin wideband radar absorbers," *IEEE Trans. Antenna Propag.*, vol. 58, no. 12, pp. 4051–4058, Dec. 2010.
- [10] G. I. Kiani, A. R. Weily, and K. P. Esselle, "A novel absorb/transmit FSS for secure indoor wireless networks with reduced multipath fading," *IEEE Microw. Wireless Compon. Lett.*, vol. 16, no. 6, pp. 378–380, Jun. 2006.

- [11] G. I. Kiani, K. L. Ford, K. P. Esselle, A. R. Weily, and C. J. Panagamuwa, "Oblique incidence performance of a novel frequency selective surface absorber," *IEEE Trans. Antenna Propag.*, vol. 55, no. 10, pp. 2931–2934, Oct. 2007.
- [12] F. Costa, A. Monorchio, and G. Manara, "Analysis and design of ultra thin electromagnetic absorbers comprising resistively loaded high impedance surfaces," *IEEE Trans. Antennas Propag.*, vol. 58, no. 5, pp. 1551–1558, May 2010.
- [13] F. Costa and A. Monorchio, "A frequency selective radome with wideband absorbing properties," *IEEE Trans. Antennas Propag.*, vol. 60, no. 6, pp. 2740–2747, Jun. 2012.
- [14] L. Sun, H. Cheng, Y. Zhou, and J. Wang, "Broadband metamaterial absorber based on coupling resistive frequency selective surface," *Opt. Exp.*, vol. 20, no. 4, pp. 4675–4680, Feb. 2012.
- [15] Y. Shang, Z. Shen, and S. Xiao, "On the design of single-layer circuit analog absorber using double-square-loop array," *IEEE Trans. Antenna Propag.*, vol. 61, no. 12, pp. 6022–6029, Dec. 2013.
- [16] Y. Shang, Z. Shen, and S. Xiao, "Frequency-selective rasorber based on square-loop and cross-dipole arrays," *IEEE Trans. Antenna Propag.*, vol. 62, no. 11, pp. 5581–5589, Nov. 2014.
- [17] C. Mias, "Frequency selective absorption using lumped element frequency selective surfaces," *Electron. Lett.*, vol. 39, no. 11, pp. 847–849, May 2003.
- [18] A. Itou, H. Ebara, H. Nakajima, K. Wada, and O. Hashimoto, "An experimental study of a $\lambda/4$ wave absorber using a frequency-selective surface," *Microw. Opt. Technol. Lett.*, vol. 28, no. 5, pp. 321–323, Mar. 2001.
- [19] B. Li and Z. Shen, "Three-dimensional bandpass frequency-selective structures with multiple transmission zeros," *IEEE Trans. Microw. Theory Techn.*, vol. 61, no. 10, pp. 3578–3589, Oct. 2013.
- [20] B. Li and Z. Shen, "Three-dimensional dual-polarized frequency selective structure with wide out-of-band rejection," *IEEE Trans. Antennas Propag.*, vol. 62, no. 1, pp. 130–137, Jan. 2014.
- [21] B. Li and Z. Shen, "Angular-stable and polarization-independent frequency selective structure with high selectivity," *Appl. Phys. Lett.*, vol. 103, pp. 171607-1–171607-4, Oct. 2013.
- [22] A. K. Rashid, B. Li, and Z. Shen, "An overview of three-dimensional frequency-selective structures," *IEEE Antennas Propag. Mag.*, vol. 56, no. 3, pp. 43–67, Jun. 2014.
- [23] B. Li and Z. Shen, "Wideband 3D frequency selective rasorber," *IEEE Trans. Antennas Propag.*, vol. 62, no. 12, pp. 6536–6541, Dec. 2014.
- [24] B. Li and Z. Shen, "3D frequency selective rasorber: Concept, theory, and design," in *Proc. Asia-Pacific Microw. Conf.*, Nanjing, China, Dec. 2015, pp. 1–3.
- [25] G. Q. Luo *et al.*, "Theory and experiment of novel frequency selective surface based on substrate integrated waveguide technology," *IEEE Trans. Antennas Propag.*, vol. 53, no. 12, pp. 4035–4043, Dec. 2005.
- [26] F. Costa, A. Monorchio, and G. Manara, "An equivalent-circuit modeling of high impedance surfaces employing arbitrarily shaped FSS," in *Proc. ICEEA*, Turin, Italy, Sep. 2009, pp. 852–855.
- [27] D. M. Pozar, *Microwave Engineering*, 4th ed. Hoboken, NJ, USA: Wiley, 2012.
- [28] N. Marcuvitz, *Waveguide Handbook*, 1st ed. New York, NY, USA: McGraw-Hill, 1951.
- [29] R. Garg, P. Bhartia, I. Bahl, and A. Ittipiboon, *Microstrip Antenna Design Handbook*. Reading, MA, USA: Artech House, 2001.



Zhongxiang Shen (M'98–SM'04) received the B.Eng. degree in electrical engineering from the University of Electronic Science and Technology of China, Chengdu, China, in 1987, the M.S. degree in electrical engineering from Southeast University, Nanjing, China, in 1990, and the Ph.D. degree in electrical engineering from the University of Waterloo, Waterloo, ON, Canada, in 1997.

From 1990 to 1994, he was with the Nanjing University of Aeronautics and Astronautics, Nanjing. In 1997, he was with Com Dev International Ltd., Cambridge, ON, as an Advanced Member of Technical Staff. He spent six months each in 1998, as a Post-Doctoral Fellow, first with the Gordon McKay Laboratory, Harvard University, Cambridge, MA, USA, and then with the Radiation Laboratory, University of Michigan, Ann Arbor, MI, USA. In 1999, he joined Nanyang Technological University, Singapore, as an Assistant Professor, where he has been an Associate Professor with the School of Electrical and Electronic Engineering since 2004. He has authored or co-authored over 150 journal papers and 140 conference papers. His current research interests include the design of small and planar antennas for various wireless communication systems, the analysis and design of frequency-selective structures, and hybrid numerical techniques for modeling RF/microwave components and antennas.

Dr. Shen is a member of the IEEE Antennas and Propagation Society and the IEEE Microwave Theory and Techniques Society. He served as the Chair of the IEEE MTT/AP Singapore Chapter and the IEEE AP-S Chapter Activities Committee from 2010 to 2014. He is currently the Secretary of the IEEE AP-S and an Associate Editor of the IEEE TRANSACTIONS ON ANTENNAS AND PROPAGATION.



bers.

Jiang Wang received the B.Eng. degree in information countermeasure technology from the Nanjing University of Science and Technology, Nanjing, China, in 2012, where he is currently pursuing the Ph.D. degree in electromagnetic field and microwave technology.

From 2014 to 2016, he was a Research Assistant with the School of Electrical and Electronic Engineering, Nanyang Technological University, Singapore. His current research interests include polarizers, frequency selective surfaces, and rasor-



Bo Li was born in Hunan, China, in 1984. He received the B.S. and Ph.D. degrees in communication engineering from the Nanjing University of Science and Technology, Nanjing, China, in 2006 and 2011, respectively.

From 2011 to 2014, he was with Nanyang Technological University, Singapore, as a Research Fellow. Since 2014, he has been with the Nanjing University of Posts and Telecommunications, Nanjing, where he has been a Professor with the School of Electronic Science and Engineering since 2015. His current research interests include RF/microwave power dividers and frequency-selective surfaces.